



Scalable fabrication of a flexible interdigital micro-supercapacitor device by *in-situ* polymerization of pyrrole into hybrid PVA-TEOS membrane

Anand I. Torvi, Balappa B. Munavalli, Satishkumar R. Naik, Mahadevappa Y. Kariduraganavar*

Department of Chemistry, Karnatak University, Dharwad 580 003, India



ARTICLE INFO

Article history:

Received 2 April 2018

Received in revised form

21 May 2018

Accepted 5 June 2018

Available online 6 June 2018

Keywords:

Micro-supercapacitor

Polypyrrole

Tetraethyl orthosilicate

Electrically conductive

Binder-free

ABSTRACT

This paper addresses the development of an electrically conductive flexible nanocomposite membrane by the incorporation of an optimum amount of pyrrole into tetraethyl orthosilicate crosslinked poly(vinyl alcohol). The incorporated pyrrole underwent *in-situ* chemical oxidation in presence of iron(III) chloride. The resulting membrane was subjected to various techniques to understand its physico-chemical properties. The nanocomposite membrane demonstrated an excellent electrical conductivity of 4.56 S cm^{-1} with a desired flexibility. The electrochemical properties of the electrode membrane were systematically investigated using cyclic voltammetry, galvanostatic charge-discharge and electrochemical impedance spectroscopy. The resulting electrode membrane exhibited a specific capacitance as high as 484 F g^{-1} at a current density of 0.1 A g^{-1} with an excellent cycle life stability. Based on its excellent electrochemical performance, we have developed both interdigital micro-supercapacitor and sandwich-type supercapacitor devices; among these, the interdigital micro-supercapacitor exhibited a specific capacitance of 51.42 F g^{-1} at 0.05 A g^{-1} , which is two times higher than that of sandwich-type supercapacitor (25.49 F g^{-1}). Furthermore, the method adopted here for the fabrication of an interdigital micro-supercapacitor device can be easily applied to large-scale fabrication of electrically conductive membranes and opens up new opportunities for flexible lightweight energy storage devices.

© 2018 Elsevier Ltd. All rights reserved.

1. Introduction

The increasing depletion of fossil fuels and the environmental problems associated with their use have forced the development of efficient, clean and sustainable sources of energy [1–3]. In pursuit of this, supercapacitors have been recognized as one of the most useful inventions among all the energy storage devices. Supercapacitors are electrochemical energy storage devices, which have a higher energy-density than conventional capacitors and higher power-density than batteries. Thus, the supercapacitors can fill the gap between the traditional capacitors and batteries [4,5]. In addition, supercapacitors generate less heat than common batteries and thereby they may have additional safety advantages. In view of this, supercapacitors have been used in wide range of applications, including, hybrid vehicles, electronics, railway transport, aviation,

actuators, voltage stabilizers, etc [6–10].

The performance of the supercapacitors is determined mainly by three factors; electrode materials, the electrolyte and the assembly technology [11]. Among the electrode materials, flexible and binder-free electrodes have shown great promise in portable and flexible electronics, for applications such as roll-up displays, photovoltaic cells and wearable devices [12,13]. In view of recent environmental awareness, interest in the selection of electrode material has been directed towards finding “green” or “greener” materials especially fluorine-free binders [14,15]. Moreover, current electronic devices are still too heavy, thick and bulky to match the flexibility requirements. Thus, there is an urgent need to develop energy storage devices that are light, thin, flexible, and have a high energy-density, high power-density and excellent cycling stability. To address this, various energy storage devices with diverse size, shape and good mechanical properties are being developed across the globe [16–23].

Prompted by the unique structural and electrical properties of

* Corresponding author.

E-mail address: mahadevappayk@gmail.com (M.Y. Kariduraganavar).

carbon, carbon-based flexible and stretchable supercapacitors are currently attracting considerable interest [24,25]. Unfortunately, the performance of carbon-based supercapacitors, usually referred as electrical double layer capacitors (EDLCs), is limited, due to their inherent low specific capacitance, and the relatively high cost of carbon nanotubes and elaborate synthetic procedures required in their manufacture would further limit their applications in large-scale fabrication [26,27]. On the other hand, pseudocapacitors developed based on transition metal oxides and conducting polymers (CPs), are redox active materials and show very high capacitance behavior [28–31]. Among these materials, conducting polymer based pseudocapacitors have demonstrated excellent performance for portable and flexible supercapacitor applications owing to their high-redox active capacitance, high conductivity and most importantly, high intrinsic flexibility. Among the conducting polymers, polypyrrole (PPy) is one of the most promising p-type materials for pseudocapacitor applications due to its unique features, including high conductivity, fast charge-discharge mechanism, high energy density, low cost and good thermal stability [32,33]. The electrochemical behavior of PPy-based electrode also depends on the electrode preparation methods and effective surface area of the active electrode. For instance, Mihranyan et al. [34] developed a porous electrode material by coating a thin PPy layer (~50 nm) on a cellulose substrate using cladophora algae and achieved a charge capacity of 33 mAh g⁻¹. Similarly, An et al. [32] synthesized a PPy-carbon aerogel composite electrode using a chemical oxidation method and obtained a specific capacitance of 433 F g⁻¹. Recently, Kumar et al. [35] enhanced the specific capacitance (395 F g⁻¹) of polypyrrole/carbon composites by varying the concentration of *p*-toluenesulfonate. A simple polymerization method was employed by Yuan et al. [36] to fabricate the PPy-coated paper. The resulting flexible composite electrode showed a capacitance of 0.42 F cm⁻² with high energy density of 1 mWh cm⁻³ at a power density of 0.27 W cm⁻³. Similarly, Xu et al. [37] developed a PPy/bacteria cellulose based flexible supercapacitor electrode with a maximum discharge capacity of 101.9 mAh g⁻¹ at a current density of 0.16 A g⁻¹. Unfortunately, these flexible supercapacitor electrodes failed to maintain the desired mechanical strength for long-term applications.

Realizing the pros and cons of the aforementioned electrode materials, we have successfully developed a flexible membrane electrode material by *in-situ* polymerization of pyrrole in tetraethyl orthosilicate (TEOS) crosslinked poly(vinyl alcohol). The electrical conductivity of the developed electrode was optimized by judiciously varying the mole ratio of oxidant to monomer, the mass ratio of pyrrole to crosslinked PVA and the reaction time. The physico-chemical properties of the resulting electrode materials were studied using Fourier transform infrared (FT-IR) spectroscopy, thermogravimetric analysis (TGA), X-ray diffraction (XRD) and scanning electron microscopy (SEM). The hydrophilicity and mechanical properties of the membranes were respectively studied using a contact angle meter and a universal testing machine (UTM). The electrochemical properties of the electrode membrane were systematically investigated using cyclic voltammetry (CV), galvanostatic charge-discharge (GCD) and electrochemical impedance spectroscopy (EIS). Based on its excellent electrochemical performance, we have fabricated interdigital micro-supercapacitor and sandwich-type supercapacitor devices using polymer membrane for the first time in the literature. The electrochemical performances of these two devices were evaluated in terms of specific capacitance, energy density and power density, etc. The results were correlated to the design used for the fabrication of devices and properties of the material. The outcome of the results clearly suggests that the interdigital micro-supercapacitor device could become potential candidate for flexible and wearable electronics.

2. Experimental

2.1. Materials

Poly(vinyl alcohol) ($M_w \sim 125000$) was procured from s. d. fine Chemicals Ltd., Mumbai, India. Pyrrole monomer, tetraethyl orthosilicate and flourine doped tin oxide (FTO) glass were purchased from Sigma-Aldrich Chemie, GmbH, Germany. Pyrrole was distilled twice under vacuum and stored in refrigerator before use. Iron(III) chloride and hydrochloric acid were procured from Thermo Fisher Scientific India Pvt. Ltd., Mumbai, India. N,N-dimethyl formamide was procured from Merck Specialities Pvt. Ltd., Mumbai, India. All the chemicals were used as received unless stated otherwise. Deionized water was used throughout the study.

2.2. Preparation of PVA-TEOS hybrid membrane

Crosslinked hybrid PVA membrane was prepared via hydrolysis of TEOS followed by condensation [38]. PVA (5 g) were dissolved in 100 ml of distilled water at 60 °C. The hot solution was filtered and to the filtrate, TEOS (5 g, 5.34 ml) and HCl (conc, 1 ml) as a catalyst were added to carry out the sol-gel reaction. The amount of TEOS and PVA was chosen based on membrane strength and flexibility of the membrane. The solution was stirred overnight at room temperature and was then cast onto a glass plate with the aid of a casting knife. The membrane was allowed to dry at room temperature for 2–3 days and subsequently peeled-off after complete drying. The dried membrane was annealed at 60 °C in an inert atmosphere so as to ensure complete crosslinking. The thickness of the membrane was measured at different points using peacock dial thickness gauge (Model G, Ozaki MFG. Co. Ltd. Japan) with an accuracy of $\pm 5 \mu\text{m}$. The average thickness was considered for calculation. The thickness of the membrane was found to be $100 \pm 5 \mu\text{m}$.

2.3. Preparation of PVA-TEOS-PPy nanocomposite membrane

The crosslinked flexible hybrid PVA membrane with a thickness of $100 \pm 5 \mu\text{m}$ was used to fabricate the composite membranes via *in-situ* chemical oxidation of pyrrole. The detailed procedure is given below.

The hybrid PVA-TEOS membrane was immersed in a mixture of N,N-dimethylformamide (DMF) and distilled water (1:2, v/v) at 25 °C. To this, pyrrole (1.45 ml) were added drop-wise over 30 min; in this way the pyrrole monomer could penetrate into the inner network of PVA-TEOS and at the same time, the hydroxyl groups of PVA could interact with pyrrole and form hydrogen bonds thus ensuring the uniform distribution of pyrrole in PVA-TEOS network. The polymerization was carried at room temperature by slowly adding ferric chloride (0.85 g) as an oxidant and hydrochloric acid (1 ml) as a dopant. The crosslinked PVA membrane slowly turned from colorless to grey and finally to black within 15 min, which revealed the successful incorporation of PPy in PVA-TEOS template (Fig. S1). The duration of the polymerization was 2 h. After polymerization, the resulting PVA-TEOS-PPy nanocomposite membranes were thoroughly washed with distilled water and immersed in 0.1 M HCl for 30 min and dried under vacuum at 40 °C.

2.4. Preparation of hydrogel-polymer electrolyte (PVA-H₂SO₄)

The PVA-H₂SO₄ electrolyte was prepared by mixing of PVA powder (6 g), H₂SO₄ (conc., 6 g) and of deionized water (60 ml). This was heated to 85 °C until the solution became clear. The resulting solution was cooled and used as an electrolyte for the preparation of devices.

2.5. Physico-chemical characterization

The reaction between PVA and TEOS, and the polymerization of pyrrole in TEOS crosslinked PVA were probed using an FTIR spectrometer (Nicolet Impact-410, USA). A thermogravimetric analyzer (TA Instruments, DSC Q20, Waters LLC, USA) was used to study the thermal stability of PVA-TEOS and PVA-TEOS-PPy nanocomposite membranes at a heating rate of 10 °C/min under a nitrogen atmosphere. The crystal structure of the nanocomposite membranes was studied at room temperature by x-ray diffraction (Bruker, D-8 Advance, Germany) with Ni-filtered Cu K α source. The diffraction was operated in the range of 5 to 60° at 40 kV and 30 mA with a scanning speed of 8°/min at an angle 2 θ . The surface morphology of the nanocomposite membranes was examined by scanning electron microscope equipped with an energy-dispersive X-ray spectrometer (EDS) (Bruker, Quantax EDS, Germany) at various magnifications. The composition of the sample was examined using an energy dispersive spectrometer and inductively coupled plasma mass spectrometer. The contact angle of the developed membranes was measured using contact angle meter (Ramehart Instrument Co., Model:400, USA). The tensile strength, elongation at break and Young's modulus of the TEOS crosslinked PVA and PVA-TEOS-PPy samples were measured at 25 °C using a universal testing machine (Hounsfield, H25KS, UK) at a cross head speed of 1 mm/min. The sizes of the specimen were 10 cm \times 2 cm.

2.6. Electrical conductivity measurement

The electrical conductivity of the composite membranes was measured with a conventional four-point probe technique (SES Instruments, DF-P-02, India) at 25 °C. The detailed procedure is given as [supplementary information \(S1\)](#).

2.7. Electrochemical performance

The electrochemical measurements were carried out using a two electrode system. The electrochemical performance of the cell was tested using an electrochemical work station (ACM Instruments, Gill AC 660, UK) and scanned over a range of -1 V to +1 V. Galvanostatic charge/discharge tests were performed using an electrochemical work station (CH Instruments Inc., CHI 608E, USA) over a potential range of -1 V to +1 V. Electrochemical impedance spectroscopy measurements were performed in the frequency range of 100 kHz to 0.01 Hz with an amplitude of 5 mV at open circuit potential.

The specific capacitance was estimated based on cyclic voltammetry (CV) and galvanostatic charge-discharge (GCD) curves using Eqs. (1) and (2), respectively:

$$C_s = \frac{\int Idv}{2m\Delta V} \quad (1)$$

$$C_s = \frac{2I\Delta t}{m\Delta V} \quad (2)$$

Similarly, energy density and power density were determined from Eqs. (3) and (4), respectively:

$$E = \frac{CV_{\max}^2}{7200} \quad (3)$$

$$P = \frac{3600E}{\Delta t} \quad (4)$$

where, C_s is the specific capacitance (F g⁻¹); $\int Idv$, the area under the curve; m , the mass of electrode; S , the scan rate (mV s⁻¹); ΔV , the potential window (V) (excluding the internal resistance, IR, drop in the case of GCD); I , the discharge current (A); Δt , the discharge time; V_{\max} , the operation potential (V); E , the energy density (Wh kg⁻¹) and P is the power density (W kg⁻¹).

2.8. Fabrication of supercapacitor devices and their electrochemical performances

Both interdigital micro-supercapacitor and sandwich-type supercapacitor devices were fabricated as illustrated in [Fig. 1](#) using a PVA-TEOS-PPy nanocomposite membrane as an electrode material.

2.8.1. Interdigital micro-supercapacitor (IMS)

The prepared PVA-TEOS-PPy nanocomposite membrane was cut into strips (fingers) and then arranged into an interdigital electrode configuration on the polyethylene terephthalate (PET) substrate as shown in [Fig. 1](#). Copper (Cu) tape as a current collector was applied at both the ends of the micro-electrodes to ensure a good electrical contact between the micro-supercapacitor and electrochemical workstation. The polymer-gel electrolyte prepared from PVA-H₂SO₄ was drop-cast in between the micro-electrodes and allowed to dry overnight, this was then sealed through lamination with another PET sheet using an iron box.

2.8.2. Sandwich-type supercapacitor (SS)

Two PVA-TEOS-PPy nanocomposite membrane strips were used as electrodes and a PVA-H₂SO₄ polymer-gel electrolyte membrane was placed in between the two electrodes as a separator. At both the ends, Cu foils were placed as a current collector and the sandwich type device sealed using PET sheets as discussed for the fabrication of interdigital micro-supercapacitor device above. [Fig. 1](#) (a and b), show photographs of the devices, (c) shows an optical microscope image of the interdigital micro-supercapacitor and (d) shows the successful coating of polypyrrole over PVA-TEOS as evidenced by the scotch tape test.

3. Results and discussion

3.1. FT-IR study

The FTIR spectra of the hybrid PVA-TEOS and PVA-TEOS-PPy composite membranes are presented in [Fig. 2](#). From the PVA-TEOS spectrum, it is noticed that a broad band was observed at around 3400 cm⁻¹ and was attributed to O-H stretching vibrations of PVA and the uncondensed silanol groups of TEOS [38,39]. The multiple bands appeared between 1000 and 1200 cm⁻¹, and were assigned to C-O and Si-O stretchings. This is expected since both Si-O and C-O stretching vibrations appear at the same frequency [40,41]. The characteristic bands appearing at 464 and 2920 cm⁻¹ are attributed to deformation vibration of Si-O-Si bending and -CH stretching vibrations, respectively [39,42].

In contrast to the above, the PVA-TEOS-PPy composite membrane exhibited the bands at around 1550 and 1500 cm⁻¹ [43,44]. These are attributed to C-C and C-N stretching vibrations of the pyrrole, respectively. The band appearing at around 1200 cm⁻¹ was attributed to stretching vibrations of pyrrole ring [45]. The bands appeared at around 790 and 1050 cm⁻¹ are attributed to C-H (out of plane ring deformation) and N-H (in-plane ring deformation) stretching vibrations, respectively [37]. All these characteristic bands indicate the presence of PPy in the PVA-TEOS template. Further, the presence of two characteristic bands of PVA-TEOS in the FT-IR spectrum of PVA-TEOS-PPy also supports the material

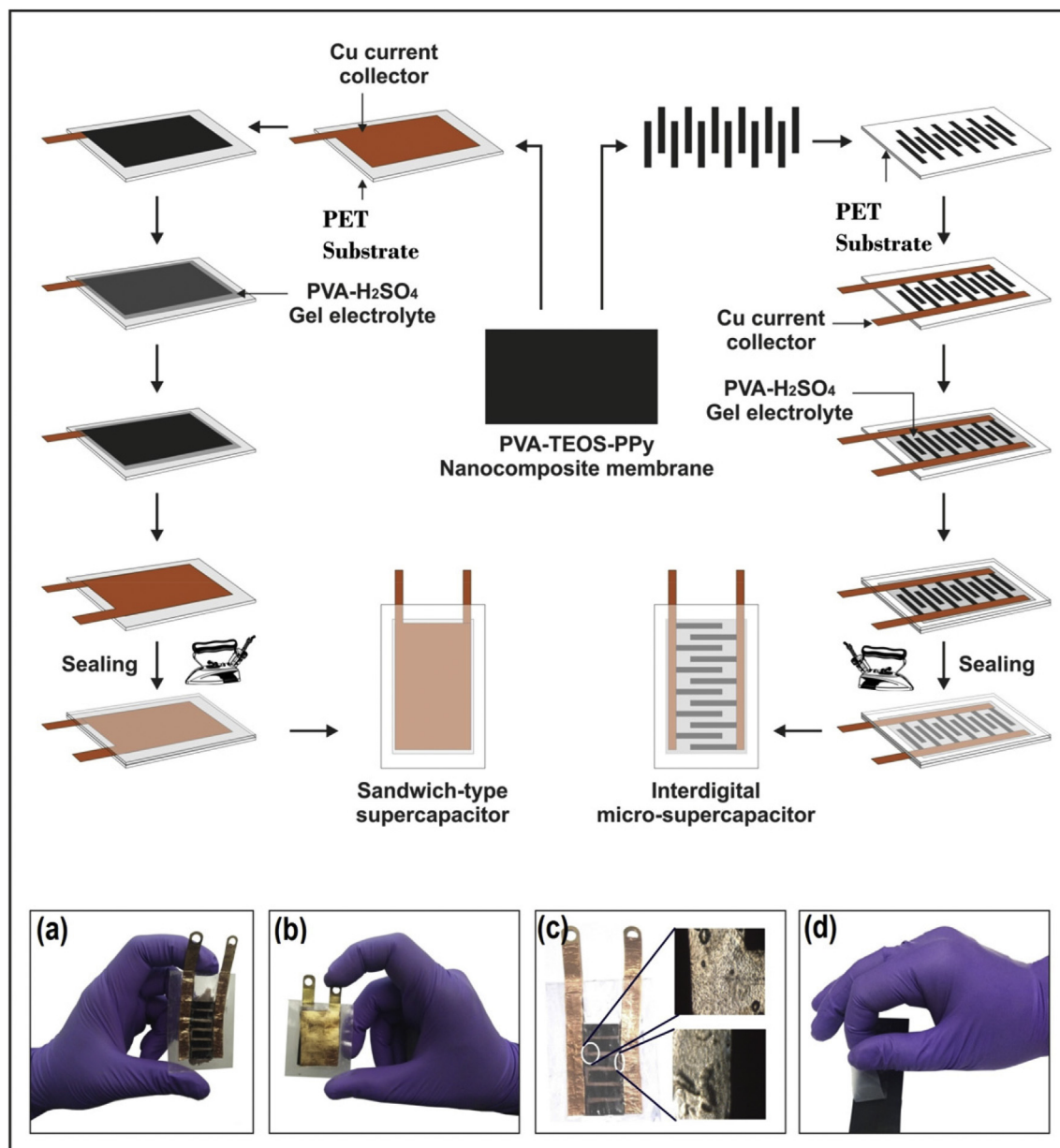


Fig. 1. Schematic representation of fabrication of interdigital micro-supercapacitor and sandwich-type supercapacitor device. (a) Interdigital micro-supercapacitor. (b) Sandwich-type supercapacitor. (c) Optical microscope image of interdigital micro-supercapacitor. (d) Successful coating of polypyrrole over PVA-TEOS membrane.

characterization. These PPy bands are in good agreement with bands reported by Xu et al. [37].

3.2. TGA study

Thermal stability and degradation behavior of PVA-TEOS and PVA-TEOS-PPy membranes were studied using TGA and the resulting thermograms are presented in Fig. S2. From the thermograms, it is observed that both the membranes underwent degradation mainly in three stages. The weight loss that occurred between ambient and 200 °C, corresponding to physically absorbed water and acid molecules. Most of the absorbed water molecules exist in a bound state rather than in a free molecular state, and hence they bound directly to the polymer chain through hydrogen bonding [46].

The second stage of decomposition of the PVA-TEOS membrane

started from 200 to 410 °C, and was attributed to the loss of side chain (TEOS) [47]. The weight loss was found to be around 37%, which closely correspond to the weight of TEOS used in the preparation of the crosslinked membrane. The third stage of weight loss occurred between 410 and 550 °C, which attributed to the loss of the PVA main chain [48]. Instead, for the PVA-TEOS-PPy membrane the second stage of decomposition occurred between 200 and 433 °C. This is due to loss of TEOS, the corresponding weight loss was found to be 28%, which closely matches the weight of TEOS employed in the preparation of composite membrane. The third stage of weight loss occurred from 433 to 550 °C. This is due to the degradation of both the PVA main chain and polypyrrole [49]. From the third stage of degradation of PVA-TEOS-PPy, it is found that PVA underwent decomposition at higher temperature than observed for the PVA-TEOS membrane. This is due to the presence of PPy in the PVA-TEOS template. The PPy layer is a more stable component,

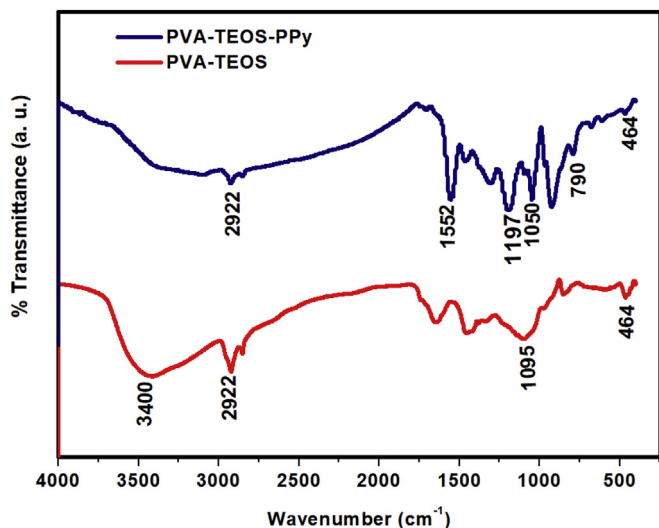


Fig. 2. FT-IR spectra of PVA-TEOS and PVA-TEOS-PPy nanocomposite membrane.

which acts as a protective barrier against the thermal degradation of PVA-TEOS [50]. The final weight residue (char) remaining in PVA-TEOS-PPy is slightly more than that of PVA-TEOS membrane. This is expected owing to presence of iron particles in the final residue.

3.3. XRD study

To understand the crystalline nature of PVA-TEOS and PVA-TEOS-PPy composite membranes, we have measured the diffraction in the reflection mode, and the data thus obtained are presented in Fig. S3. It is clear that hybrid PVA-TEOS membrane exhibited a sharp peak at $2\theta = 20^\circ$ and a broad peak at around $2\theta = 26^\circ$. These two peaks relate to the semicrystalline and amorphous nature of PVA-TEOS membrane, respectively. The broad peak that corresponded to the amorphous nature of PVA-TEOS was significantly increased upon polymerization of pyrrole. This is apparently due to presence of PPy chains at the interplanar spacing [51] and thus, it is concluded that crystalline behaviour of PVA-TEOS was suppressed by the incorporation of PPy chains in PVA-TEOS matrix.

3.4. Surface morphology and EDAX analysis

The surface morphology of hybrid PVA-TEOS and its composite membrane was analyzed using scanning electron microscopy and the images with different magnifications thus obtained are presented in Fig. 3. From the images (a-c), it can be seen that the surface of the PVA-TEOS membrane appears reasonably clean and has a sheet-like structure. However, when polypyrrole was incorporated, the clean sheet-like morphology was dramatically changed to a highly ordered wrinkle topography [52]. This is mainly due to an establishment of strong hydrogen bonding between the $-\text{OH}$ groups of PVA-TEOS and the pyrrole. In view of this, the adhesive property was greatly increased and consequently the thermal properties of the resulting nanocomposite membrane improved as supported by the thermogravimetric analysis [53,54]. For higher magnifications (g-i), we noticed small globular features ranging from 50 to 100 nm in size. These could be due to the close network of polypyrrole nanoparticles and thereby the polypyrrole was distributed evenly across the PVA-TEOS template. We take this to signify that the polypyrrole was distributed at a nanoscale level within the PVA-TEOS matrix [55].

To further confirm the incorporation of PPy in PVA-TEOS matrix, we have measured the elemental analysis using EDAX analyzer. The data thus obtained are presented in Fig. S4, together with the elements and their weight% (inset Table 1). It is observed that the elements such as C, N, O, Si and Cl were detected in the composite membrane. The presence of Si and O elements is due to the incorporation of TEOS as crosslinker in PVA. The appearance of N is attributed to the incorporation of polypyrrole in PVA-TEOS network. The appearance of 7.91% of Cl is due to the presence of dopant (HCl) and oxidant (FeCl_3) used in the preparation of membrane. All these elements confirm the successful incorporation of polypyrrole into PVA-TEOS matrix through polymerization.

3.5. Electrical conductivity study

In order to optimize the electrode material so as to achieve the highest electrical conductivity, three sets of protocols were carried out. In set-I, pyrrole was oxidized in the presence of the PVA-TEOS template by varying the mole ratio of FeCl_3 and measuring the electrical conductivity of all the membranes; the results are given in Table 1. It was found that membrane with 0.25:1 mole ratio of FeCl_3 :pyrrole demonstrated an excellent conductivity. Thus, the feeding mass ratio of pyrrole:PVA was varied in set-II. The electrical conductivity of the resulting membranes is also included in Table 1, among the data, the membrane with 1.5:1 mass ratio of pyrrole:PVA exhibited the highest electrical conductivity. Based on these data, we have fixed the mass ratio of pyrrole:PVA (1.5:1) in set-III and varied the duration of oxidation from 10 min to 12 h. It is found that membrane oxidized for 2 h duration demonstrated an excellent electrical conductivity. Thus, we have achieved the highest electrical conductivity of the nanocomposite membrane by optimizing the mole ratio of FeCl_3 :pyrrole, mass ratio of pyrrole:PVA and the reaction time. The resulting membrane demonstrated an electrical conductivity as high as 4.56 S cm^{-1} , much higher than found for PPy cellulose fibers ($0.0001\text{--}1 \text{ S cm}^{-1}$) [35,56,57], pure PPy film (1.14 S cm^{-1}) [58], PPy film (0.01 S cm^{-1}) [59], cladophora cellulose based PPy membrane ($\sim 1 \text{ S cm}^{-1}$) [34], and polypyrrole/lignosulfonate (PPy/LGS) coated cotton fabrics (3.03 S cm^{-1}) [60]. To further demonstrate the efficiency, this membrane was used as a connector for an LED display device (see supplementary material Fig. S5). The display shows very good intensity in terms of readability of the text, indicating that resulting membrane could find potential applications in the area of flexible electronic devices.

3.6. Electrochemical performance of PVA-TEOS-PPy nanocomposite

The electrochemical performance of the PVA-TEOS-PPy nanocomposite membrane was evaluated using cyclic voltammetry at different scan rates as shown in Fig. 4a. At all scan rates, CV curves exhibited roughly rectangular shapes, which is indicative of good capacitance behavior and small equivalent series resistance (ESR) [37,55]. Based on the CV curves, we have calculated the specific capacitance at different scan rates using Eq. (1). The results are presented in Fig. 4b. It is observed that the maximum specific capacitance of 518 F g^{-1} was achieved at a scan rate of 10 mV s^{-1} and it decreased to 120 F g^{-1} when the scan rate reached 120 mV s^{-1} . The decrease in specific capacitance with increasing scan rate is mainly due to inaccessibility of electrons in the electrode material, suggesting that redox transitions were not sustainable at a higher scan rate [61]. The resulting specific capacitance of PVA-TEOS-PPy nanocomposite membrane developed here is superior to that of PPy based membranes reported elsewhere [62,63].

The electrochemical performance of PVA-TEOS-PPy

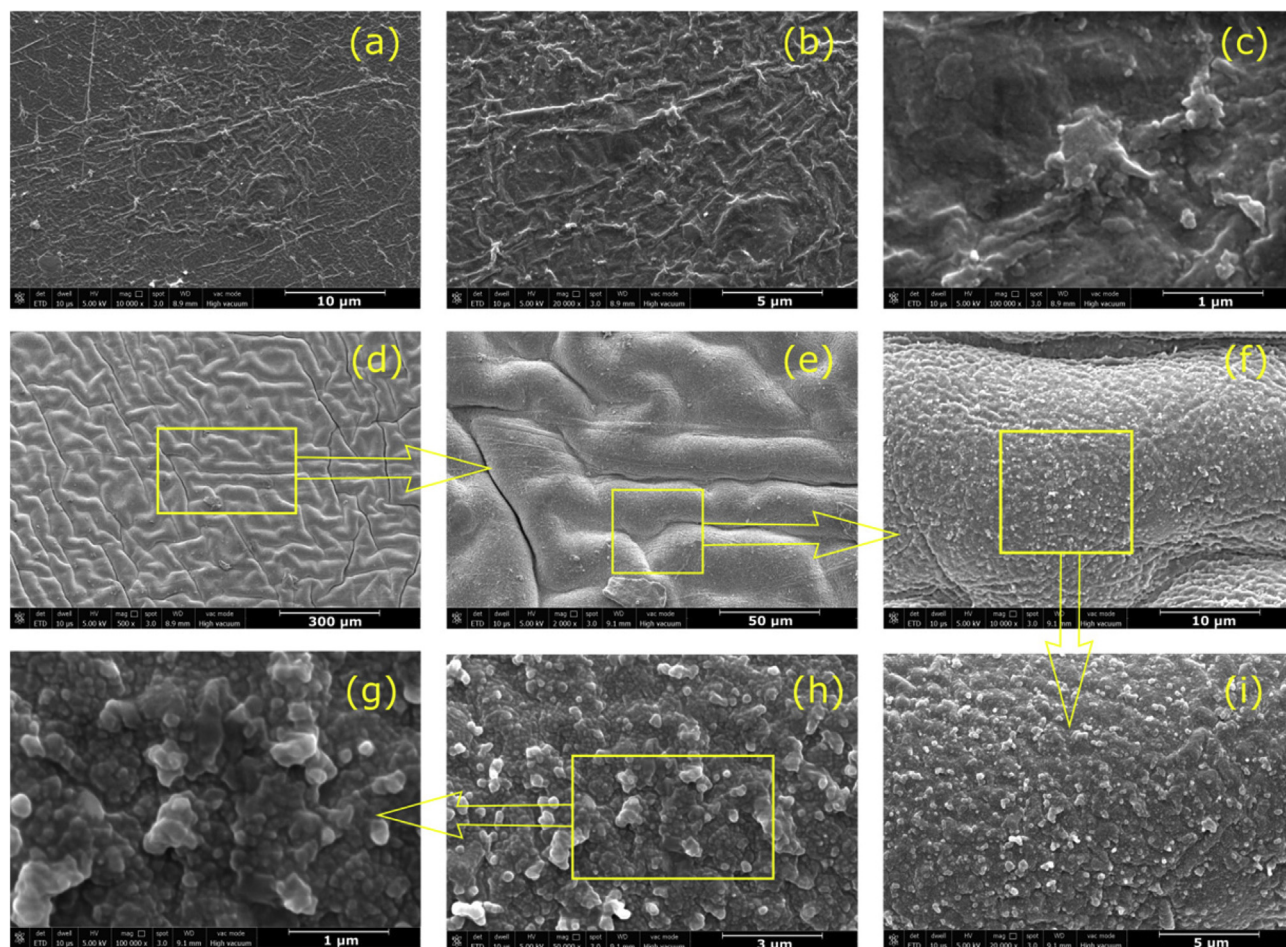


Fig. 3. SEM images of (a–c) PVA-TEOS, and (d–i) PVA-TEOS-PPy nanocomposite membranes.

Table 1
The electrical conductivity of PVA-TEOS-PPy nanocomposite membrane achieved through optimization of reaction parameters. Molar ratio of FeCl_3 :Pyrrole (set-I), mass ratio of Pyrrole:PVA (set-II), and variation of reaction time (set-III).

Set-I		Set-II		Set-III		
FeCl_3 :Pyrrole (molar ratio)	Electrical conductivity (S cm^{-1})	Pyrrole:PVA (mass ratio)	Electrical conductivity (S cm^{-1})	Pyrrole:PVA (mass ratio)	Time variation	Electrical conductivity (S cm^{-1})
0.125:1	1.257	0.25:1	0.1664	1.5:1	10 min.	1.4573
0.25:1	1.551	0.5:1	0.5556	1.5:1	30 min.	2.9809
0.5:1	0.728	1:1	1.6934	1.5:1	1 h.	3.6863
0.75:1	0.309	1.5:1	3.154	1.5:1	2 h.	4.5652
1:1	0.048	2:1	2.4917	1.5:1	3 h.	2.15
–	–	4:1	1.3499	1.5:1	6 h.	1.5512
–	–	–	–	1.5:1	12 h.	0.9111

nanocomposite was further examined by galvanostatic charge-discharge (GCD) technique. Fig. 4c displays the charge-discharge curves of PVA-TEOS-PPy nanocomposite at current densities of 0.1, 0.2, 0.5, 1 and 2 A g^{-1} . It is observed that all the curves are symmetrical in nature; this confirms the superior reversible redox reactions and excellent supercapacitive properties of the PVA-TEOS-PPy nanocomposite membrane. The GCD curves show a deviation from a triangular shape, suggesting that the developed electrode exhibited redox behaviour. This might be due to a pseudocapacitance contributed from the Faradaic reaction of PPy. The specific capacitance values of PVA-TEOS-PPy calculated from its charge-discharge curves using Eq. (2) are plotted as a function of

current density as shown in Fig. 4d from this plot, it is observed that the specific capacitance decreased monotonously with increasing the current density. The nanocomposite membrane developed demonstrated an excellent specific capacitance as high as 484 F g^{-1} at 0.1 A g^{-1} . This value is much higher than those reported for PPy, CNT and graphene based supercapacitors [52,61,64–66].

Electrochemical impedance spectroscopy (EIS) was employed to measure the charge transfer resistance of PVA-TEOS-PPy nanocomposite electrode at 5 mV amplitude over a frequency range of 100 kHz to 0.01 Hz. The Nyquist plot is drawn between the real (Z') and imaginary (Z'') parts of the impedance data as shown in Fig. 4e. The resulting Nyquist plot is divided into two frequency regions: a

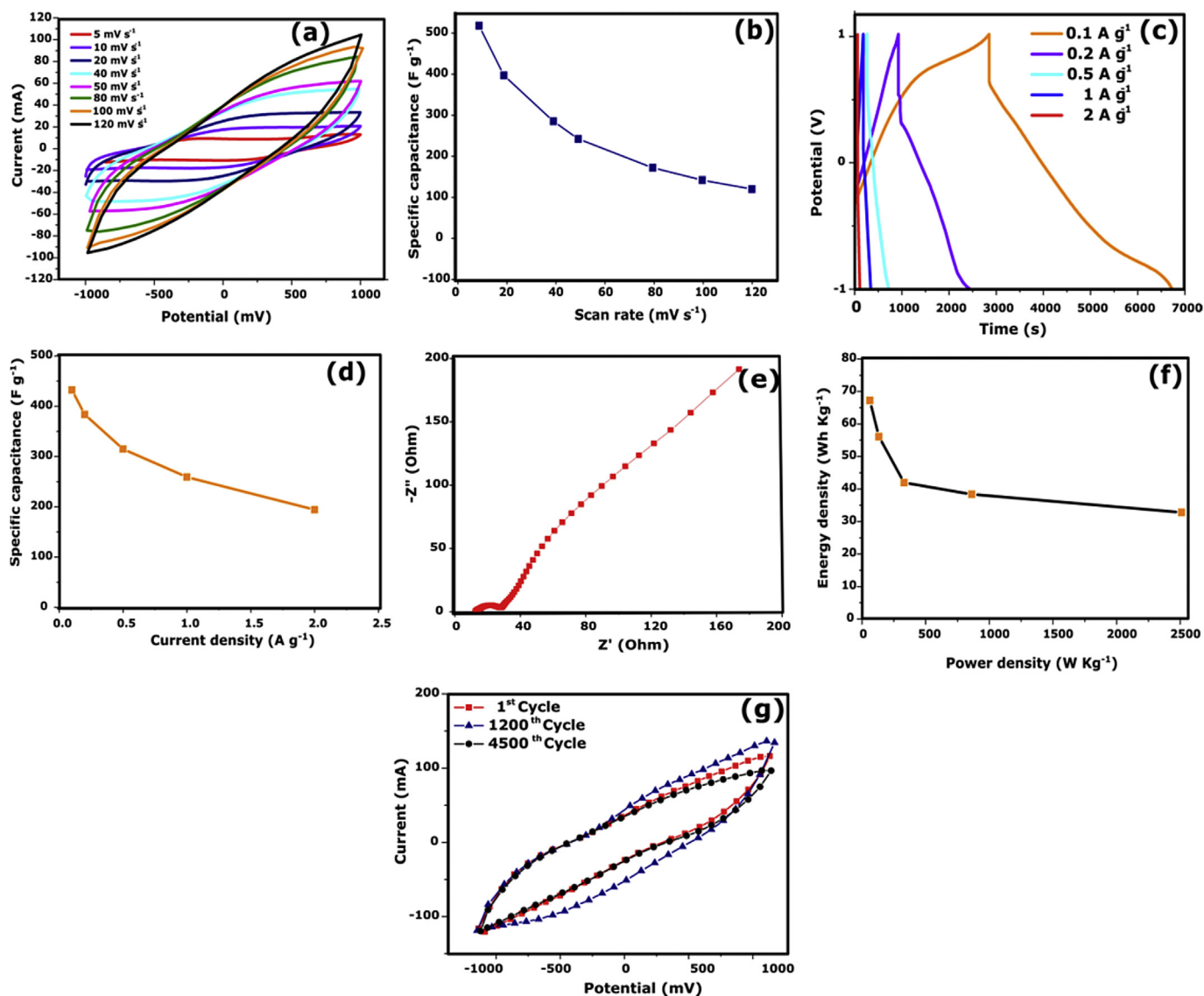


Fig. 4. Electrochemical characterization of PVA-TEOS-PPy nanocomposite membrane. (a) Cyclic voltammograms of PVA-TEOS-PPy nanocomposite membrane at different scan rates in 1 M H₂SO₄. (b) Variation of specific capacitance with scan rate. (c) Charge-discharge curves of PVA-TEOS-PPy nanocomposite membrane at different current densities. (d) Specific capacitance of PVA-TEOS-PPy nanocomposite membrane as a function of current density. (e) Nyquist plot of PVA-TEOS-PPy nanocomposite membrane. (f) Ragone plot of PVA-TEOS-PPy nanocomposite. (g) Stability curves of the PVA-TEOS-PPy membrane for the 1st, 1200th and 4500th cycles.

characteristic semicircle observed at high frequency region and an inclined portion at low frequency, this clearly indicates the existence of ideal capacitor behavior [67]. The equivalent circuit model of PVA-TEOS-PPy membrane is proposed as shown in Fig. S6. The R_s and R_{ct} are the solution resistance and charge transfer resistance, respectively. R_{des} represents the resistance of ion desorption from the nanomaterials. A constant phase element (Q_{dl}) was used to represent the double-layer capacitance at the electrode/electrolyte interface. In view of the in-homogeneity or roughness at the interface, a constant phase element was used instead of a capacitor, where Q_{ps} represents pseudocapacitive charging [68]. The values of R_s , R_{ct} , R_{des} and Q_{dl} are found to be 12.75, 14.1, 3.02 Ω and 0.22802 $\times 10^3$ F, respectively.

To assess the performance of a supercapacitor, both energy density and power density play important role, energy density represents the amount of energy stored per unit mass, whereas the power density describes how fast the energy is released. To demonstrate this, the Ragone plot of energy density versus power

density is shown in Fig. 4f. The nanocomposite electrode developed here exhibited an energy density of 67.22 Wh kg⁻¹ at a power density of 61.82 W kg⁻¹. The power density was improved to 2510 W kg⁻¹ with an energy density of 32.77 Wh kg⁻¹, indicating that the electrode retained an energy density of about 50%. These values are superior to the values reported for PPy based symmetric systems [60,69–71]. Based on the results, we ascertain that PVA-TEOS-PPy nanocomposite membrane electrode exhibited an excellent energy density and power output, which could be of use as a potential material for a high-performance supercapacitor.

Fig. 4g shows the stability curves of the PVA-TEOS-PPy membrane for the 1st, 1200th and 4500th cycles. It is observed that the specific capacitance increased from the 1st cycle to 1200th cycles, and then decreased from the 1200th to 4500th cycles. The increased specific capacitance of PVA-TEOS-PPy electrode in the first 1200th cycles is due to a self-activation process [72]. The capacitance retention was about 95% even for 4500 cycles. These results suggest that the PVA-TEOS-PPy electrode membrane demonstrated an

outstanding cycle performance as compared, for example, to PPy based supercapacitors reported in the literature [35,73–75].

3.7. Electrochemical performance of interdigital and sandwich-type devices

To assess the electrochemical performance, the newly designed and fabricated interdigital micro-supercapacitor and sandwich-type supercapacitor devices were subjected to cyclic voltammetry, galvanostatic charge-discharge technique and electrochemical impedance spectroscopy. As shown in Fig. 5a and b, both interdigital and sandwich-type supercapacitor devices show elliptical shape curves at all scan rates with no apparent redox peaks, suggesting that both the devices exhibited typical EDLC-type behaviour [76]. Among these two devices, the interdigital micro-supercapacitor (Fig. 5a) showed a current value up to 150 mA, which is almost three times higher than that of the sandwich-type supercapacitor (Fig. 5b). This clearly suggests that the interdigital micro-supercapacitor has more rapid charge transport and exhibits a higher rate performance compared to the sandwich-type supercapacitor. Similarly, a charge-discharge study was carried out in the potential range between -1 V and $+1$ V at a current density of 0.05 A g^{-1} (Fig. 5c). It is noticed that both the devices showed the triangular charge-discharge curves. At fixed current density of 0.05 A g^{-1} , the specific capacitances of the interdigital micro-

supercapacitor and sandwich-type supercapacitors were found to be 51.42 and 25.49 F g^{-1} , respectively. Between the two, the interdigital micro-supercapacitor exhibited almost double the capacitance compared to the sandwich-type supercapacitor. This is mainly due to the unique design (pattern) employed for the fabrication of interdigital micro-supercapacitor, which minimizes the pathway for ion diffusion between the electrolyte and electrode material. In addition to this, the micro-scale architecture of the device results in a significant reduction of the mean ionic diffusion pathway between the two microelectrodes. Thus, the interdigital micro-supercapacitors have several advantages over the conventional sandwich-type supercapacitors. First, having both electrodes in the same plane is compatible with on-chip integration. Second, the travelling distance of the ions in the electrolyte is a major performance factor in supercapacitors, which can be very well controlled and shortened while eliminating the necessity of a separator, which is indispensable in the sandwich-type supercapacitors to prevent the electrical shorting [77]. Third, the interdigital structure could potentially be extended to three dimensions, which allows loading more material per unit area while leaving the mean ionic diffusion path unaffected. Thus, this architecture has the potential to achieve a high power density and high energy density in a small footprint [78,79].

EIS measurements were also carried out for both interdigital and sandwich-type devices at a sinusoidal signal of 5 mV in the

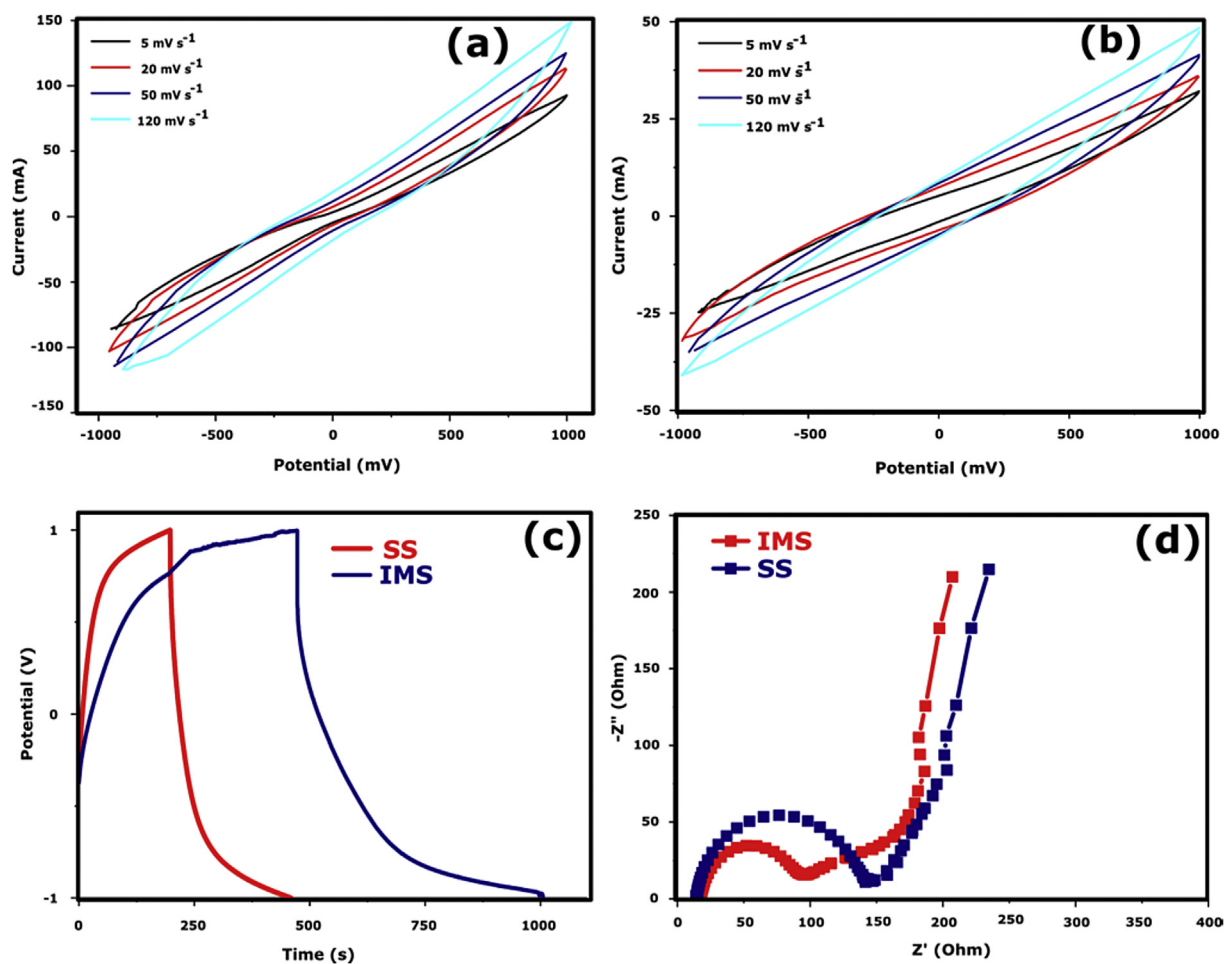


Fig. 5. Electrochemical performance of supercapacitor devices. Cyclic voltammograms of (a) interdigital micro-supercapacitor and (b) sandwich-type supercapacitor at different scan rates. (c) Charge-discharge curves of interdigital micro-supercapacitor and sandwich-type supercapacitor at fixed current density of 0.05 A g^{-1} . (d) Nyquist plot of sandwich-type and interdigital micro-supercapacitors.

frequency range of 100 kHz to 0.01 Hz. Fig. 5d shows the corresponding Nyquist plots of both the devices. A nearly vertical Nyquist plot was observed in both the devices at low frequency range, which indicates an ideal capacitor behaviour owing to the fast diffusion of ions across the electrode material. In the high-frequency region, it is possible to measure the equivalent series resistance from the extrapolated intersection of the curve with real axis of impedance Z' , which corresponds to zero for Z'' . The estimated equivalent series resistance values of the interdigital and sandwich-type devices were found to be 85 and 150 Ω , respectively. Consequently, the specific capacitance of the interdigital micro-supercapacitor device was almost two times higher (51.42 F g^{-1}) than that of sandwich-type supercapacitor (25.49 F g^{-1}). This infers that the interdigital micro-supercapacitor device developed here with a unique design by judiciously choosing the hybrid flexible material demonstrated an excellent performance as a supercapacitor.

Finally, we have also calculated the energy density and power density of supercapacitor devices. The interdigital micro-supercapacitor exhibited extremely high energy density of 7.14 Wh kg^{-1} with a power density of 47.60 W kg^{-1} as compared to the sandwich-type supercapacitor, which has an energy density of just 3.5 Wh kg^{-1} with a power density of 49.0 W kg^{-1} . Thus, we can achieve a significant increase in supercapacitor performance when scaling down the electrode dimensions to the micro-scale using interdigital micro-supercapacitor.

4. Conclusions

A simple method is adopted to prepare the electrically conductive flexible membrane using TEOS crosslinked PVA as a hybrid substrate via *in-situ* polymerization of pyrrole. It is evident from the study that polypyrrole was successfully incorporated into a crosslinked PVA template. The electrical conductivity of the resulting PVA-TEOS-PPy membrane was optimized by varying the reaction parameters, such as molar ratio of oxidant to monomer, mass ratio of pyrrole to PVA-TEOS and the reaction time. The optimized composite membrane showed an excellent electrical conductivity as high as 4.56 S cm^{-1} with improved thermal stability. The developed PVA-TEOS-PPy membrane exhibited an excellent electrochemical performance with a specific capacitance of 484 F g^{-1} at 0.1 A g^{-1} in 1 M H_2SO_4 electrolyte, while retaining the cycle life stability of 95% as evidenced from the retention of capacitance even after 4500 cycles. Electrochemical measurements have clearly shown that the PVA-TEOS-PPy nanocomposite could be used as a good electrode material for micro-supercapacitor. Considering its flexibility, high specific capacitance and good cycle life stability, we further developed a new flexible, low cost and easily fabricated interdigital micro-supercapacitor device with a unique design using the PVA-TEOS-PPy nanocomposite as an electrode material and its performance was systematically investigated. It exhibits a specific capacitance of 51.42 F g^{-1} , which is almost two times higher than that of the sandwich-type supercapacitor (25.49 F g^{-1}) at a current density of 0.05 A g^{-1} . Based on its electrochemical performance, the newly designed and fabricated interdigital micro-supercapacitor could be a promising device for supercapacitor applications.

Acknowledgments

Authors (B. B. Munavalli and S. R. Naik) sincerely thank the UGC, New Delhi, for awarding the fellowships to carry out the research work under the RFSMS scheme. The authors also wish to thank the

UGC, New Delhi, for providing the financial support under the CPEPA Program [Grant No. 8-2/2008(NS/PE)]. This work is also supported by the DST-PURSE-Phase-II Program, Department of Science & Technology, New Delhi [Grant No. SR/PURSE PHASE-2/13(G)]. The authors remain grateful to Dr. Fred J. Davis, Professor, Department of Chemistry, University of Reading, Reading, UK, for doing the language corrections in the manuscript.

Appendix A. Supplementary data

Supplementary data related to this article can be found at <https://doi.org/10.1016/j.electacta.2018.06.034>.

References

- [1] B.E. Conway, *Electrochemical Supercapacitors: Scientific Fundamentals and Technological Applications*, Springer, New York, 1999.
- [2] B.E. Conway, W. Pell, Double-layer and pseudocapacitance types of electrochemical capacitors and their applications to the development of hybrid devices, *J. Solid State Electrochem.* 7 (2003) 637–644.
- [3] A. Burke, Why, how, and where is the technology, *J. Power Sources* 91 (2000) 37–50.
- [4] P. Simon, Y. Gogotsi, Materials for electrochemical capacitors, *Nat. Mater.* 7 (2008) 845–854.
- [5] P. Simon, Y. Gogotsi, Capacitive energy storage in nanostructured carbon–electrolyte systems, *J. Acc. Chem. Res.* 46 (2012) 1094–1103.
- [6] Q. Zhou, C. Jia, X. Ye, Z. Tang, Z. Wan, A knittable fiber-shaped supercapacitor based on natural cotton thread for wearable electronics, *J. Power Sources* 327 (2016) 365–373.
- [7] H. Jin, L. Zhou, C.L. Mak, H. Huang, W.M. Tang, H.L.W. Chan, High-performance fiber-shaped supercapacitors using carbon fiber thread (CFT)@polyaniline and functionalized CFT electrodes for wearable/stretchable electronics, *Nano Energy* 11 (2015) 662–670.
- [8] Z. Zhang, X. Zhang, W. Chen, Y. Rasim, W. Salman, H. Pan, Y. Yuan, C. Wang, A high-efficiency energy regenerative shock absorber using supercapacitors for renewable energy applications in range extended electric vehicle, *Appl. Energy* 178 (2016) 177–188.
- [9] A. Frilli, E. Meli, D. Nociolini, L. Pugi, A. Rindi, Energetic optimization of regenerative braking for high speed railway systems, *Energy Convers. Manag.* 129 (2016) 200–215.
- [10] A. Rufer, D. Hotellier, P. Barrade, A supercapacitor-based energy storage substation for voltage compensation in weak transportation networks, *IEEE Trans. Power Deliv.* 19 (2004) 629–636.
- [11] S.L. Zhang, N. Pan, Supercapacitors performance evaluation, *Adv. Energy Mater* 5 (2015) 1401401–1401420.
- [12] C. Shen, Y. Xie, B. Zhu, M. Sanghadasa, Y. Tang, L. Lin, Wearable woven supercapacitor fabrics with high energy density and load-bearing capability, *Sci. Rep.* 7 (2017) 14324.
- [13] Z. Liu, H.I. Wang, A. Narita, Q. Chen, Z. Mics, D. Turchinovich, M. Kläui, M. Bonn, K. Müllen, Photo switchable micro-supercapacitor based on a diarylethene-graphene composite film, *J. Am. Chem. Soc.* 139 (2017) 9443–9446.
- [14] R. Lopez-Chavez, A.K. Cuentas-Gallegos, The effect of binder in electrode materials for capacitance improvement and EDLC binder-free cell design, *J. New. Mater. Electrochem. Syst* 16 (2013) 197–202.
- [15] B. Dyatkin, V. Presser, M. Heon, M. Lukatskaya, M. Beidaghi, Y. Gogotsi, Development of a green supercapacitor composed entirely of environmentally friendly materials, *Chemsuschem* 6 (2013) 2269–2280.
- [16] J. Yu, F. Xie, Z. Wu, T. Huang, J. Wu, D. Yan, C. Huang, L. Li, Flexible metallic fabric supercapacitor based on graphene/polyaniline composites, *Electrochim. Acta* 259 (2018) 968–974.
- [17] S. Zheng, X. Tang, Z.S. Wu, Y.Z. Tan, S. Wang, C. Sun, H.M. Cheng, X. Bao, Arbitrary-shaped graphene-based planar sandwich supercapacitors on one substrate with enhanced flexibility and integration, *ACS Nano* 11 (2017) 2171–2179.
- [18] J.J.A. Espinoza, H.P. deOliveira, Flexible supercapacitors based on a ternary composite of polyaniline/polypyrrole/graphite on gold coated sandpaper, *Electrochim. Acta* 274 (2018) 200–207.
- [19] H.Y. Li, Y. Yu, L. Liu, L. Liu, Y. Wub, One-step electrochemically expanded graphite foil for flexible all-solid supercapacitor with high rate performance, *Electrochim. Acta* 228 (2017) 553–561.
- [20] Y. Bu, M. Cao, Y. Jiang, L. Gao, Z. Shi, X. Xiao, M. Wang, G. Yang, Y. Zhou, Y. Shen, Ultra-thin bacterial cellulose/poly(ethylenedioxythiophene) nanofibers paper electrodes for all-solid-state flexible supercapacitors, *Electrochim. Acta* 271 (2018) 624–631.
- [21] M. Zhang, Y. Liu, M. Hu, H. Wei, Y. Gao, Spiral wire-type stretchable all-solid-state supercapacitors based on $\text{MnO}_2/\text{graphene}/\text{Ni}$ wires, *Electrochim. Acta* 256 (2017) 44–51.

- [22] M. Mo, C. Chen, H. Gao, M. Chen, D. Li, Wet-spinning assembly of cellulose nanofibers reinforced graphene/polypyrrole microfibers for high performance fiber-shaped supercapacitors, *Electrochim. Acta* 269 (2018) 11–20.
- [23] Z. Lin, X. Qiao, Coral-like Co_3O_4 Decorated N-doped carbon particles as active materials for oxygen reduction reaction and supercapacitor, *Sci. Rep.* 8 (2018) 1802.
- [24] A. Scalia, F. Bella, A. Lamberti, S. Bianco, C. Gerbaldi, E. Tresso, C. Fabrizio Pirri, A flexible and portable power pack by solid-state supercapacitor and dye-sensitized solar cell integration, *J. Power Sources* 359 (2017) 311–321.
- [25] L. Zolin, J.R. Nair, D. Beneventi, F. Bella, M. Destro, P. Jagdale, I. Cannavaro, A. Tagliaferro, D. Chaussy, F. Geobaldo, C. Gerbaldi, A simple route toward next-gen green energy storage concept by nanofibres-based self-supporting electrodes and a solid polymeric design, *Carbon* 107 (2016) 811–822.
- [26] A.G. Pandolfo, A.F. Hollenkamp, Carbon properties and their role in supercapacitors, *J. Power Sources* 157 (2006) 11–27.
- [27] E. Frackowiak, F. Beguin, Carbon materials for the electrochemical storage of energy in capacitors, *Carbon* 39 (2001) 937–950.
- [28] M.B. Sassin, C.N. Chervin, D.R. Rolison, J.W. Long, Redox deposition of nanoscale metal oxides on carbon for next-generation electrochemical capacitors, *Acc. Chem. Res.* 46 (2013) 1062–1074.
- [29] M.C. Zhi, J.L. Xiang, M. Li, N. Wu, Nanostructured carbon-metal oxide composite electrodes for supercapacitors: a review, *Nanoscale* 5 (2013) 72–88.
- [30] M. Kalaji, P.J. Murphy, G.O. Williams, The study of conducting polymers for use as redox supercapacitors, *Synth. Met.* 102 (1999) 1360–1361.
- [31] T. Liu, L. Finn, M. Yu, H. Wang, T. Zhai, X. Lu, Polyaniline and polypyrrole pseudocapacitor electrodes with excellent cycling stability, *Nano Lett.* 14 (2014) 2522–2527.
- [32] H. An, Y. Wang, X. Wang, L. Zheng, X. Wang, L. Yi, Polypyrrole/carbon aerogel composite materials for supercapacitor, *J. Power Sources* 195 (2010) 6964–6969.
- [33] J. Wang, Y. Xu, J. Wang, X. Du, Toward a high specific power and high stability polypyrrole supercapacitors, *Synth. Met.* 161 (2011) 1141–1144.
- [34] A. Mihranyan, G. Nystrom, A. Razaq, M. Strømme, L. Nyholm, Ultrafast all-polymer paper-based batteries, *Nano Lett.* 161 (2009) 3635–3639.
- [35] A. Kumar, R.K. Singh, H.K. Singh, P. Srivastava, R. Singh, Enhanced capacitance and stability of p-toluenesulfonate doped polypyrrole/carbon composite for electrode application in electrochemical capacitors, *J. Power Sources* 246 (2014) 800–807.
- [36] L. Yuan, B. Yao, B. Hu, K. Huo, W. Chen, J.J. Zhou, Polypyrrole-coated paper for flexible solid-state energy storage, *Energy Environ. Sci.* 6 (2013) 470–476.
- [37] J. Xu, L. Zhu, Z. Bai, G. Liang, L. Liu, D. Fang, W. Xu, Conductive polypyrrole-bacterial cellulose nanocomposite membranes as flexible supercapacitor electrode, *Org. Electron.* 14 (2013) 3331–3338.
- [38] M.Y. Kariduraganavar, S.S. Kulkarni, A.A. Kittur, Preparation separation of water-acetic acid mixture through poly(vinyl alcohol)-silicone based hybrid membranes, *J. Membr. Sci.* 246 (2005) 83–93.
- [39] R. Bryskova, D. Pencheva, G.M. Kale, U. Lad, T. Kantardjiev, Synthesis, characterisation and antibacterial activity of PVA/TEOS/Ag-Np hybrid thin films, *J. Colloid Interface Sci.* 349 (2010) 77–85.
- [40] D. Mullera, C.R. Rambob, L.M. Portoc, W.H. Schreinerd, G.M.O. Barraa, Structure and properties of polypyrrole/bacterial cellulose nanocomposites, *Carbohydr. Polym.* 94 (2013) 655–662.
- [41] R. Gangopadhyay, A. De, An electrochemically synthesized conducting semi-IPN from polypyrrole and poly(vinyl alcohol), *J. Mater. Chem.* 12 (2002) 3591–3598.
- [42] M. Dirican, M. Yanilmaz, K. Fu, O. Yildiz, H. Kizil, Y. Hu, X. Zhang, Carbon-confined PVA-derived silicon-silica-carbon nanofiber composites as anode for lithium-ion batteries, *J. Electrochem. Soc.* 161 (2014) A2197–A2203.
- [43] R. Gangopadhyay, A. De, G. Ghosh, Polyaniline–poly(vinyl alcohol) conducting composite: material with easy processability and novel application potential, *Synth. Met.* 123 (2001) 21–31.
- [44] M. Omastová, M. Trchová, J. Kovářová, J. Stejskal, Synthesis and structural study of polypyrroles prepared in the presence of surfactants, *Synth. Met.* 138 (2003) 447–455.
- [45] Y. Tian, F. Yang, W. Yang, Redox behavior and stability of polypyrrole film in sulfuric acid, *Synth. Met.* 156 (2006) 1052–1056.
- [46] I.O. Honma, N.T. Sugimoto, S. Nomura, H. Nakajima, A sol-gel derived organic-inorganic hybrid membrane for intermediate temperature PEFC, *Fuel Cell.* 2 (2002) 52–58.
- [47] F. Quan, L.L. Chen, Y. Xia, Q. Ji, Structure and properties of PVA/SiO₂ interpenetrating polymer network materials prepared by the sol-gel method, *Polym. Polym. Compos.* 17 (2009) 97–100.
- [48] A. Mihranyan, G. Nystrom, A. Razaq, T. Lindstrom, L. Nyholm, M.A. Strømme, Nanocellulose, polypyrrole composite based on microfibrillated cellulose from wood, *J. Phys. Chem.* 114 (2010) 4178.
- [49] B. Bideau, J. Bras, S. Saini, C. Daneault, E. Loranger, Mechanical and antibacterial properties of a nanocellulose-polypyrrole multilayer composite, *Mater. Sci. Eng. C* 69 (2016) 977–984.
- [50] C.R. Rambo, D.O.S. Recouvreur, L.M. Porto, G.M.O. Barra, Chemical in-situ polymerization of polypyrrole on bacterial cellulose nanofibers, *D. Müller, Synth. Met.* 161 (2011) 106–111.
- [51] R.E. Partch, S.G. Gangoli, E. Matijevic, W. Cai, S. Araj, Conducting polymer composites: surface-induced polymerization of pyrrole on iron(III) and cerium(IV) oxide particles, *J. Colloid Interface Sci.* 144 (1991) 27–35.
- [52] M.R. Aufan, Y. Sumi, S. Kim, J.Y. Lee, Facile synthesis of conductive polypyrrole wrinkle topographies on polydimethylsiloxane via a swelling-deswelling process and their potential uses in tissue engineering, *ACS Appl. Mater. Interfaces* 7 (2015) 23454–23463.
- [53] H.G. Premakshi, A.M. Sajjan, M.Y. Kariduraganavar, Development of pervaporation membranes using chitosan and titanium glycine- N,N-dimethylphosphonate for dehydration of isopropanol, *J. Mater. Chem., A* 3 (2015) 3952–3961.
- [54] H.G. Premakshi, M.Y. Kariduraganavar, G.R. Mitchell, Development of composite anion-exchange membranes using poly(vinyl alcohol) and silica precursor for pervaporation separation of water–isopropanol mixtures, *RSC Adv.* 6 (2016) 11802–11814.
- [55] J.P. Wang, Y.L. Xu, J. Wang, X.F. Du, F. Xiao, J.B. Li, High charge-discharge rate polypyrrole films prepared by pulse current polymerization, *Synth. Met.* 160 (2010) 1826–1831.
- [56] J.H. Johnston, F.M. Kelly, J. Moraes, T. Borrmann, D. Flynn, Conducting polymer composites with cellulose and protein fibres, *Curr. Appl. Phys.* 6 (2006) 587–590.
- [57] M.J. Richardson, J.H. Johnston, T. Borrmann, Electronic properties of intrinsically conducting polymer-cellulose based composites, *Curr. Appl. Phys.* 6 (2006) 462–465.
- [58] D. Wang, Y.X. Li, Z. Shi, H.L. Qin, L. Wang, X.F. Pei, J. Jin, Spontaneous growth of free-standing polypyrrole films at an air/ionic liquid interface, *Langmuir* 26 (2010) 14405–14408.
- [59] K.T. Song, J.Y. Lee, H.D. Kim, D.Y. Kim, S.Y. Kim, C.Y. Kim, Solvent effects on the characteristics of soluble polypyrrole, *Synth. Met.* 110 (2000) 57–63.
- [60] L. Zhu, L. Wu, Y. Sun, M. Li, J. Xu, Z. Bai, G. Liang, L. Liu, D. Fang, W. Xu, Cotton fabrics coated with lignosulfonate (PPy/LGS)-doped polypyrrole for flexible supercapacitor electrodes, *RSC Adv.* 4 (2014) 6261–6266.
- [61] W. Liu, X. Yan, J. Lang, C. Peng, Q. Xue, Flexible and conductive nanocomposite electrode based on graphene sheets and cotton cloth for supercapacitor, *J. Mater. Chem.* 22 (2012) 17245–17253.
- [62] S.S. Shinde, G.S. Gund, V.S. Kumbhar, B.H. Patil, C.D. Lokhande, Novel chemical synthesis of polypyrrole thin film electrodes for supercapacitor application, *Eur. Polym. J.* 49 (2013) 3734–3739.
- [63] S.C. Zhitomirsky, Electrodeposition and capacitive behavior of films for electrodes of electrochemical supercapacitors, *Nanoscale Res. Lett.* 5 (2010) 518–523.
- [64] K.F. Babu, S.P. Siva Subramanian, M.A. Kulandainathan, Functionalisation of fabrics with conducting polymer for tuning capacitance and fabrication of supercapacitor, *Carbohydr. Polym.* 94 (2013) 487–495.
- [65] B. Yue, C. Wang, X. Ding, G.G. Wallace, Polypyrrole coated nylon lycra fabric as stretchable electrode for supercapacitor applications, *Electrochim. Acta* 68 (2012) 18–24.
- [66] M. Pasta, F.L. Mantia, L. Hu, H.D. Deshazer, Y. Cui, Aqueous supercapacitors on conductive cotton, *Nano Res.* 3 (2010) 452–458.
- [67] Z.F. Li, H. Zhang, Q. Liu, L. Sun, L. Stanciu, Fabrication of high-surface-area graphene/polyaniline nanocomposites and their application in supercapacitors, *J. ACS Appl. Mater. Inter.* 5 (2013) 2685–2691.
- [68] M. Arunkumar, A. Paul, Importance of electrode preparation methodologies in supercapacitor applications, *ACS Omega* 2 (2017) 8039–8050.
- [69] S. Peng, L. Fan, W. Rao, Z. Bai, W. Xu, J. Xu, Bacterial cellulose membranes coated by polypyrrole/copper oxide as flexible supercapacitor electrodes, *J. Mater. Sci.* 196 (2017) 1930–1942.
- [70] J. Xu, D. Wang, Y. Yuan, W. Wei, L. Duan, L. Wang, W. Xu, Polypyrrole/reduced graphene oxide coated fabric electrodes for supercapacitor application, *Org. Electron.* 24 (2015) 153–159.
- [71] J. Xu, D. Wang, L. Fan, Y. Yuan, W. Wei, R. Liu, S. Gu, W. Xu, Fabric electrodes coated with polypyrrole nanorods for flexible supercapacitor application prepared via a reactive self-degraded template, *Org. Electron.* 26 (2015) 292–299.
- [72] X. Lu, D. Zheng, T. Zhai, Z. Liu, Y. Huang, S. Xie, Y. Tong, Facile synthesis of large-area manganese oxide nanorod arrays as a high-performance electrochemical supercapacitor, *Energy Environ. Sci.* 4 (2011) 2915–2921.
- [73] A. Mihranyan, A. Razaq, L. Nyholm, M. Sjödin, M. Strømme, Paper-based energy-storage devices comprising carbon fiber-reinforced polypyrrole-cladophora nanocellulose composite electrodes, *Adv. Energy Mater.* 2 (2012) 445–454.
- [74] H. Olsson, G. Nystrom, M. Stromme, M. Sjödin, L. Nyholm, Cycling stability and self-protective properties of a paper-based polypyrrole energy storage device, *Electrochem. Commun.* 13 (2011) 869–871.
- [75] V. Khomenko, E. Raymundo-Pinero, E. Frackowiak, F. Beguin, High-voltage asymmetric supercapacitors operating in aqueous electrolyte, *Appl. Phys. A* 82 (2006) 567–573.
- [76] N. Choudhary, M. Patel, Y.H. Ho, N.B. Dahotre, W. Lee, J.Y. Hwang, W. Choi, Directly deposited MoS₂ thin film electrodes for high performance supercapacitors, *J. Mater. Chem. A* 3 (2015) 24049–24054.
- [77] J.J. Yoo, Ultrathin planar graphene supercapacitors, *Nano Lett.* 11 (2011) 1423–1427.
- [78] T.S. Arthur, D.J. Bates, N. Cirigliano, D.C. Johnson, P. Malati, J.M. Mosby, E. Perre, M.T. Rawls, A.L. Prieto, D. Bruce, Three-dimensional electrodes and battery architectures, *MRS Bull.* 36 (2011) 523–531.

- [79] C. Shen, X. Wang, W. Zhang, F. Kang, A high-performance three-dimensional micro supercapacitor based on self-supporting composite materials, *J. Power Sources* 196 (2011) 10465–10471.

Nomenclature

TEOS: Tetraethyl orthosilicate

PVA: Poly(vinyl alcohol)

EIS: Electrochemical impedance spectroscopy

CV: Cyclic voltammetry

GCD: Galvanostatic charge-discharge

EDLC: Electrochemical double layer capacitors

MOs: Metal oxides

CPs: Conducting polymers

CNTs: Carbon nanotubes

PPy: Polypyrrole

FTO: Fluorine doped tin oxide

M_w: Molecular weight

DMF: N,N-Dimethylformamide

FTIR: Fourier transform infrared spectroscopy

TGA: Thermogravimetric analysis

SEM: Scanning electron microscope

UTM: Universal testing machine

EDAX: Energy-dispersive X-ray spectroscopy

XRD: X-ray diffraction

mA: Milliampere

Mm: Micrometer

Cu: Copper

θ : Theta (degree)

V: Volt

A: Ampere

cm: Centimeter

σ : Conductivity

F: Farad

kg: Kilogram

E: Energy density

P: Power density

PET: Poly(ethylene terephthalate)

LED: Light emitting diode

ESR: Equivalent series resistance

KHz: Kilo Hz

SS: Sandwich-type supercapacitor

IMS: Interdigital micro-supercapacitor